WARSAW UNIVERSITY OF TECHNOLOGY Index 351733
FACULTY OF CIVIL ENGINEERING
COMMITTEE FOR CIVIL AND WATER ENGINEERING
POLISH ACADEMY OF SCIENCES ISSN 1230-2945

DOI: 10.24425/ace.2026.157470

ARCHIVES OF CIVIL ENGINEERING

Vol. LXXII ISSUE 1 2026

pp. 223–239

Research paper

Dynamic responses of Schwedler dome and geodesic dome to wind load

Urszula Radoń[1], Waldemar Szaniec[2], Urszula Pawlak[3], Paweł Zabojszcza[4]

Abstract: The paper analyses the effect of wind load on the dynamic responses of two domes. This is not a standard design situation, therefore static analysis alone is not sufficient. The main objective of this paper is to compare the results obtained from the application of dynamic equilibrium equations and those obtained from static analysis. The authors wanted to determine the sensitivity of the domes to the wind load. Inertial forces and dynamic equilibrium equations were taken into account in the calculations. The integration of the equations of motion was performed using the unconditionally stable version of Newmark's method. Numerical calculations were performed using the author's MES3D program. Two patterns and two heights of single-layer steel domes were considered, i.e. a low Schwedler dome and a high geodesic dome. The structural stability and damping capacity of the domes were compared. The analysis includes a modal study to determine the natural frequencies and their corresponding vibration modes. Then, the displacements and accelerations of the keystone of both domes were assessed.

Keywords: modal analysis, wind load, Newmark method, Schwedler dome, geodesic domes

[1]Prof., Kielce University of Technology, Faculty of Civil Engineering and Architecture, Kielce, Poland, e-mail: zmbur@tu.kielce.pl, ORCID: 0000-0002-7842-7480
[2]DSc., Kielce University of Technology, Faculty of Civil Engineering and Architecture, Kielce, Poland, e-mail: waldek.szaniec@tu.kielce.pl, ORCID: 0000-0003-4397-1563
[3]DSc., Kielce University of Technology, Faculty of Civil Engineering and Architecture, Kielce, Poland, e-mail: u.pawlak@tu.kielce.pl, ORCID: 0000-0002-1454-6181
[4]DSc., Kielce University of Technology, Faculty of Civil Engineering and Architecture, Kielce, Poland, e-mail: pawelzab@tu.kielce.pl, ORCID: 0000-0002-4131-3906

1. Introduction

Steel roof covers in large-span structures are characterized by relatively high stiffness with low material consumption, but they are susceptible to variable loads. Current research of steel roof covers are primarily focuses on stability problems, dynamic performance, topology optimization. Mashrah et al. [1] proposed a numerical method to assess the stability of single-layer latticed domes under static loads. Additionally, they provided design recommendations to improve stability and stress distribution. In order to determine the forms of stability loss and the critical load values, researchers use both deterministic and probabilistic descriptions. In paper [2] show stability of single-layer latticed structures with correlated initial geometric imperfection model using conditional autoregressive model. Influence of randomness of buckling coefficient on the reliability index is described in [3]. Optimization problems of steel roof covers are often discussed in scientific papers. In the article [4], the use of the meta-heuristic algorithm Charged System Search (CSS) allowed the creation of geodesic dome configurations. In the optimization process, nodes and structural elements are automatically generated, allowing for fast and efficient verification of the structure. In the work [5], the authors use the surrogate finite element method, in which they take into account neural networks based on physics-informed neural networks to solve the problems of optimizing the size, shape and topology of single-layer domes. A different approach to the problem of optimizing the topology of nonlinear single-layer domes is presented in the article [6]. The authors use an algorithm inspired by the electron rush around the nucleus of atoms in a molecule, called the electro-search algorithm. Despite the limitations related to the poor efficiency of solving discrete structure optimization problems, the algorithm shows good performance for reference functions. The performance analysis was performed using statistical tests. Dynamic response of the steel roof covers to seismic, wind, impact load is widely described in [7–10]. In the study conducted by Nie et al. [7], the damage modes of single-layer spherical lattice structures subjected to earthquake loading were investigated through a comprehensive analysis using incremental dynamic analysis methods. Zhu et al. [8] established energy-based criteria for dynamic damage and collapse of steel shell lattice structures, supported by experimental studies and numerical simulations. Li et al. [9] identified three distinct damage mechanisms of single-layer spherical lattice structures subjected to impact loading and provided valuable design recommendations. Lu et al. [10] used the autoregressive (AR) method to simulate wind loads on single-layer cylindrical lattice structures. They applied explicit finite element analysis to investigate the dynamic collapse behaviour induced by wind action. Their study focused on the collapse process and the underlying mechanisms by analysing the internal forces in the structural members and the maximum nodal displacements. Alizadeh et al. [11] investigated the static and dynamic stability of spherical shell lattice structures under wind loading by simulating variable wind pressure on the shell surface, using mathematical models and theoretical calculations to estimate the critical dynamic loads. Their findings showed that the dynamic load-bearing capacity of truss shell structures under wind action is significantly lower than their static load-bearing capacity. Dynamic effects can lead to oscillations and deformations, resulting in partial or complete structural failure. Notable examples include the collapse of the roof of the Olympic Stadium in Montreal (Figure 1a) and the failure of the radar dome and antenna structure in Reno, Nevada, USA (Figure 1b), both attributed to strong wind gusts.

(a) (b)

Fig. 1. (a) Olimpic Stadium Montreal, Roof failure under wind action [12], (b) Reno Nevada radar dome damage [13]

The our considerations included the oldest covers used in civil engineering, i.e., domes. These structures have been known since 27 BCE, i.e., since the Romans used stone blows to cover their palaces. In modern times, concrete or steel is used to build domes. The most popular ones are steel domes, which are lighter than other conventional forms. This kind of structures is the best solution for long-span roofs. Steel domes can be divided into standard (traditional domes) and non-standard ones (tensegrity cable-strut domes [14–16]). The standard domes are built with rods assembled in single-layer or double-layer grids. Depending on the arrangement of the rods, the single-layer structures can be divided into several groups (dome patterns). The most common are five of them, i.e., Ribbed dome [17–19], Kiewitt dome [20–24], Lamella dome [25], Schwedler dome [25–27] and geodesic dome [28–31]. The last two are most interesting due to their geometry. In the paper these pattern of domes are analyzed. The Schwedler pattern is used to build a low-elevation dome. On the other hand, the geodesic pattern is used to build a high-elevation dome.

This paper is a continuation of the considerations contained in the article [26]. In the current version minor changes have been introduced in the modeling of the structure. The eigenproblem has been resolved again. Next the authors decided to check how each of the domes would behave under the influence of sudden changes in the load value. In the context of climate change, the occurrence of sudden, strong gusts of wind is no longer an isolated case. The load applied in this way does not meet the conditions of a statically applied load, dynamic effects appear in the structure. In such a situation, inertia forces must be taken into account in the calculations and the dynamic equilibrium equations must be solved. The integration of the equations of motion was carried out using the unconditionally stable version of Newmark's method. Numerical calculations were performed using the author's MES3D program. Domes differ in geometry. The Schwedler dome is a low structure characterized by low stiffness. For this dome, the height-to-span ratio is 0.04. The opposite of the Schwedler dome is the geodesic dome, whose height-to-span ratio is 0.31.

2. Materials and methods

The domes are located in the Beskid Niski Mountains in Poland. Loads were determined in accordance with the relevant standards [N.1–N.3]. The detailed static and strength analysis of the domes was published in the article [27].

2.1. Schwedler dome

The first example is the Schwedler dome measuring 25 meters in diameter and 1 meter high. The reinforced concrete ring is placed on 16 reinforced concrete columns 10 meters high, which constitute a rigid base of the structure. The dome itself consists of 81 nodes and 224 rods (Figure 2). The structural elements of the dome were assumed to be steel pipes with Young's modulus $E = 210$ GPa, yield strength $f_y = 355$ MPa, and Poisson's ratio $\nu = 0.3$. Three groups of members were modeled for the dimensioning of the structure: meridians, parallels and diagonals. Each meridian is 2.511 meters long and the lengths of the parallels are 4.877 meters, 3.908 meters, 2.934 meters, 1.958 meters and 0.979 meters, respectively. The roof covering is made of tubular steel bars and glass panels. The cross-sections of the individual bar groups are as follows: parallel (RO 273 × 8), meridian (RO 127 × 8.8) and diagonal (RO 82.5 × 6.3).

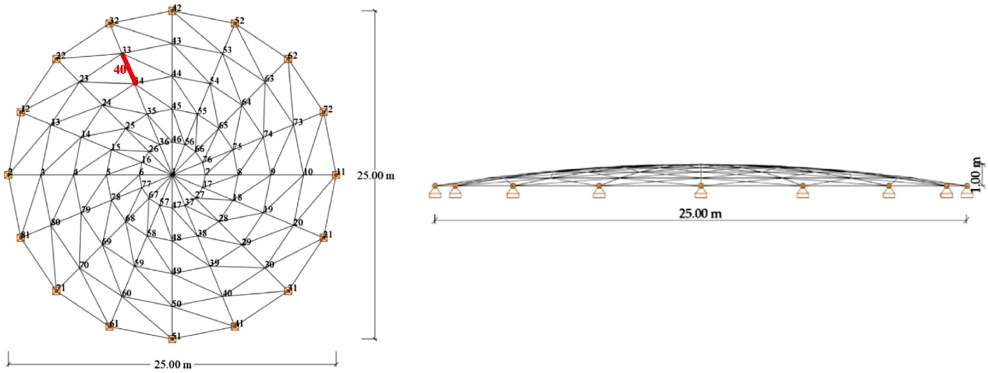

(a) (b)

Fig. 2. Schwedler dome: (a) geometry plan view; (b) side view

2.2. Geodesic dome

The second example is the geodesic dome measuring 21 meters in diameter and 6.5 meter high. The dome is mounted on a reinforced concrete ring, which is a rigid structure that simulates boundary conditions. The ring is supported by 20 reinforced concrete columns with a height of 10 meters. The dome consists of 51 nodes and 130 rods (Figure 3). The structural elements of the dome were assumed to be steel pipes with Young's modulus $E = 210$ GPa, yield strength $f_y = 235$ MPa, and Poisson's ratio $\nu = 0.3$. The current standards [N.1–N.3] were the basis for collecting loads. All structural rods were made of RO 101.6 × 8.

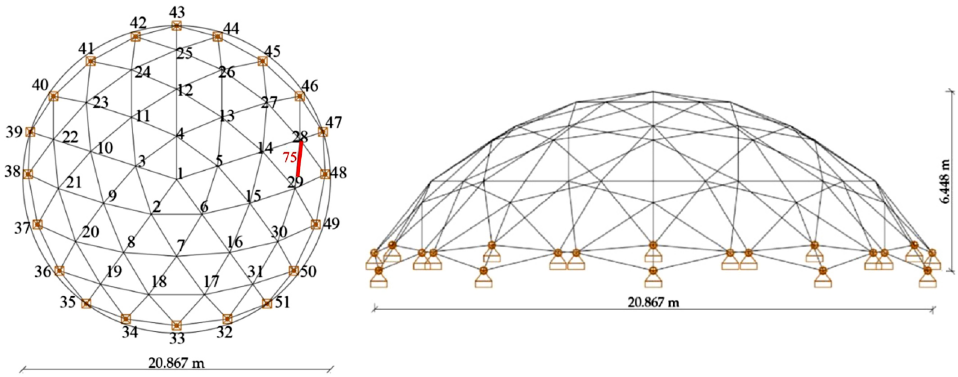

(a) (b)

Fig. 3. Geodesic dome: (a) geometry plan view; (b) side view

2.3. Numerical model of the load and the structure

Addressing the actual impact of wind on single-layer domes presents a considerable challenge for designers. The random nature of wind necessitates several simplifying assumptions, one of the most critical being the presumption that the load acts statically. For circular domes, the Eurocode [N.3] recommends taking surface loads acting in a direction normal to the surface of the sphere. These values are constant in any arc formed by cutting the dome with a surface perpendicular to the wind direction (Figure 4).

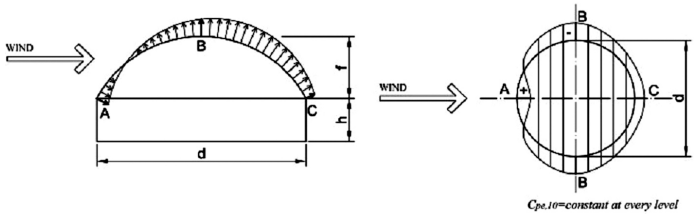

Fig. 4. Distribution of the normal wind pressure on a circular dome [Eurocode N3]

Based on the geometry of the dome and its position, the values of the force coefficients at points A, B and C are determined. Values at the remaining points are determined using a parabolic approximation. It is assumed that a load of constant value, measured for the centre of gravity of each surface element, acts on the individual surface elements. Triangular elements are used to transfer the load from the dome surface to the nodes. In case the area is 4-node, the load is divided into two equal parts and then transferred to the grid nodes using triangular elements with different grid pattern. This is shown schematically in Figure 5. This approach did not introduce the additional errors associated with using a triangular grid.

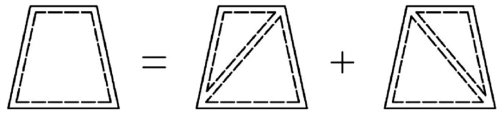

Fig. 5. Assumed load pattern

Both domes were modelled as spatial frames. The bars were rigidly connected to each other at the nodes, each dome was supported in a pinned manner. The mass of the bars was modelled as uniformly distributed while the mass of the roof covering and equipment was modelled as concentrated in the nodes.

In many engineering problems, treating the wind as a static load is sufficient. In these static calculations, the wind speed is a constant. Unfortunately, in the case of flexible structures, gusts of wind can cause vibrations of significant amplitudes. In order to calculate the wind force, it is then necessary to correctly determine the relationship describing how the wind speed changes depending on time and position. The wind speed relationship can be presented as the sum of the average wind speed and random fluctuations. Random fluctuations of wind speed are characterized in the frequency domain by the spectral density function. In the dynamic analyses we use a wind model based on the Fourier series, which presents the variability of wind speed over time as a sum of several simple sinusoidal waves, i.e. harmonic components. Each of them has its own frequency, amplitude, and initial phase. Each harmonic component is responsible for a different "rhythm" of wind changes – e.g. one for slow fluctuations, another for fast vibrations. By adding them all together, we obtain a wind course close to the real one. Such a model is useful, for example, in the dynamic analysis of steel roof coverings, where it is necessary to take into account the action of wind varying over time in a more orderly and predictable form. In our paper the parameters for each sinusoidal wave are calculated using Davenport spectral density function [32–36].

In the modal analysis of both domes we account for the influence of axial forces S in the bars on the obtained natural frequencies.

$$\left[\mathbf{K}_{\mathrm{L}} + \mathbf{K}_{\mathrm{G}}(\mathrm{S})\omega_i^2\mathbf{M}\right]\mathbf{w}_i = 0 \tag{2.1}$$

where: $\mathbf{K}_{\mathrm{L}}$ is the linear stiffness matrix, $\mathbf{K}_{\mathrm{G}}(\mathrm{S})$ is the geometric stiffness matrix, $\mathbf{M}$ is the mass matrix, ω_i is the eigenfrequency, $\mathbf{w}_i$ is the vector called the eigenvector of the i-th mode of vibration.

The set of eigenvectors forms an eigenmatrix $\mathbf{W}$:

$$\mathbf{W} = [\mathbf{w_1}, \mathbf{w_2}, \ldots, \mathbf{w}_d] \tag{2.2}$$

where: d is the number of dynamic degrees of freedom.

For numerical integration of the equations of motion under load, the unconditionally stable variant of Newmark's method [37] was selected, which does not introduce amplitude errors into the calculations. Basic equations of motion we can written as:

$$\mathbf{M}\ddot{\mathbf{q}} + \mathbf{C}\dot{\mathbf{q}} + (\mathbf{K}_{\mathrm{L}} + \mathbf{K}_{\mathrm{G}}(\mathrm{S}))\,\mathbf{q} = \mathbf{P} \tag{2.3}$$

where: $\mathbf{C}$ is the damping matrix, $\mathbf{q}$ is the vector of nodal displacements, $\mathbf{P}$ is the vector of nodal load.

During the calculations we observe the displacements and accelerations of the keystone of both domes in the vertical direction (z axis). Additionally, we check the values of axial forces in the most stressed bars.

Equations of motion in modal coordinates

$$\mathbf{W}^{\mathbf{T}}\mathbf{M}\mathbf{W}\ddot{\boldsymbol{\eta}} + \mathbf{W}^{\mathbf{T}}\mathbf{C}\mathbf{W}\dot{\boldsymbol{\eta}} + \mathbf{W}^{\mathbf{T}}\left(\mathbf{K}_{\mathrm{L}} + \mathbf{K}_{\mathrm{G}}(\mathrm{S})\right)\mathbf{W}\boldsymbol{\eta} = \mathbf{W}^{\mathbf{T}}\mathbf{P} \tag{2.4}$$

where: modal damping factors ζ_i $(i = 1, 2, \ldots d)$ can be determined from

$$\mathbf{W}^{\mathbf{T}}\mathbf{C}\mathbf{W} = \mathrm{diag}\,\{2\zeta_i\omega_i\}$$

2.4. Description of the programme MES3D

The MES3D module designed by the authors was used for dynamic calculations. The MES3D program was created at the Kielce University of Technology. It was written in Object Pascal in the Lazarus IDE environment. The application is based on the classic finite element method, in calculations we can use flat and spatial bar elements and 3- and 4-node shell elements and transition elements used to transfer loads to nodes. The MES3D program allows obtaining static solutions, natural vibrations and dynamic calculations – integration of motion equations. The influence of large axial forces can be taken into account in them by using a geometric matrix. The MES3D software can be connected to probabilistic calculation software's (e.g. NumpressExplore [38]), which was used in [39, 40]. By default, in the standard mode it is an interactive program. This applies especially to the visualization of obtained solutions. It is constantly being developed in terms of computational possibilities. Modal analysis was performed based on Lapack library procedures, developed in 2006-2012 at the universities of Tennessee, Berkeley and Denver [41].

3. Results and discussion

The first stage of calculations was dedicated to modal analysis. The results presented in the Table 1 show significantly higher natural frequencies for the geodesic dome compared to the Schwedler dome. The natural frequencies are determined by the stiffness of the structure, which is much lower in the case of the Schwedler dome. This characteristic of the Schwedler dome is also evident in the structure's response to the impact of a wind gusts.

Based on the book, [42], Table 5.2, p. 22 the dimensionless damping coefficient γ for steel structures is assumed to be 0.02. In the Rayleigh damping model, the constants κ and μ were chosen to obtain 1% critical damping for the two modal shapes. Assuming the dimensionless damping factor γ at the level of 0.02 results in a modal damping factor ζ value of 0.01.

The damping matrix $\mathbf{C}$ is described as:

$$\mathbf{C} = \mu \cdot \mathbf{M} + \kappa(\mathbf{K}_{\mathrm{L}} + \mathbf{K}_{\mathrm{G}}\,(\mathrm{S})) \tag{3.1}$$

For the two natural frequencies ω_i, ω_j important in the task, the parameters μ and κ were determined from the solution of the system of equations.

$$\begin{cases} \kappa\omega_i + \dfrac{\mu}{\omega_i} = \gamma \\ \kappa\omega_j + \dfrac{\mu}{\omega_j} = \gamma \end{cases} \tag{3.2}$$

For the geodesic dome the calculations are as follows
$\omega_1 = 110.13$ rad/s; $\omega_2 = 112.50$ rad/s
$\kappa = 0.0001$; $\mu = 1.1143$
where: ω_1 describes the symmetrical form of vibrations, while ω_2 describes the antisymmetrical form.

For the Schwedler dome the calculations are as follows
$\omega_1 = 21.65$ rad/s; $\omega_3 = 35.94$ rad/s
$\kappa = 0.0003$; $\mu = 0.2702$
where: ω_1 describes the antisymmetrical form of vibrations, while ω_3 describes the symmetrical form.

In the case of using the first ten vibration frequencies, the calculation results of the parameters μ and κ did not change significantly and are $\kappa = 0.0001$, $\mu = 1.1816$ for the Schwedler dome, and $\kappa = 0.0003$, $\mu = 0.2923$ for the geodesic dome, respectively.

Table 1. Results of modal analysis for Schwedler dome and geodesic dome

Mode	Frequency		Modal damping factor	
	Schwedler dome f_i/ω_i	Geodesic dome f_i/ω_i	Schwedler dome ζ_i	Geodesic dome ζ_i
1	3.45 Hz / 21.65 rad/s	17.53 Hz / 110.13 rad/s	0.009487	0.010566
2	3.45 Hz / 21.65 rad/s	17.91 Hz / 112.50 rad/s	0.009487	0.010577
3	5.72 Hz / 35.94 rad/s	17.91 Hz / 112.50 rad/s	0.009150	0.010577
4	5.75 Hz / 36.13 rad/s	19.51 Hz / 122.61 rad/s	0.009159	0.010675
5	5.75 Hz / 36.13 rad/s	19.69 Hz / 123.73 rad/s	0.009159	0.010689
6	6.31 Hz / 39.62 rad/s	19.69 Hz / 123.73 rad/s	0.009353	0.010689
7	6.31 Hz / 39.62 rad/s	19.84 Hz / 124.63 rad/s	0.009353	0.010702
8	6.82 Hz / 42.86 rad/s	19.84 Hz / 124.63 rad/s	0.009581	0.010702
9	7.21 Hz/ 45.32 rad/s	20.25 Hz/ 127.23 rad/s	0.009779	0.010741
10	7.21 Hz/ 45.32 rad/s	20.25 Hz/ 127.23 rad/s	0.009779	0.010741

It is worth noting the different form of deformation of both considered structures. In the case of the Schwedler structure (Figure 6), there is a clear tendency to global deformation (taking into account the entire structure at the same time), while in the case of the geodesic dome (Figure 7), local bar deformations dominate. In the case of the Schwedler dome, the first mode of vibration is antisymmetric, while in the case of the geodesic dome, it is symmetrical.

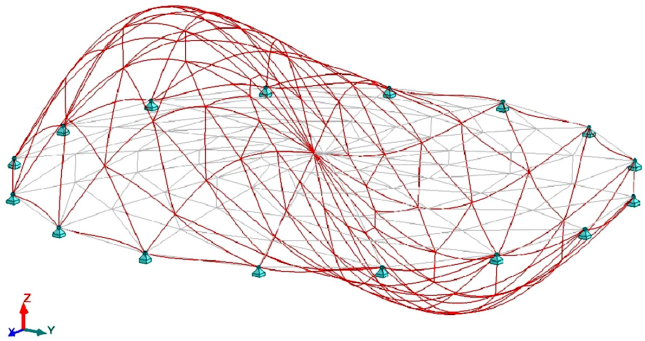

Fig. 6. Graphic illustration of the first mode of vibration of Schwedler dome

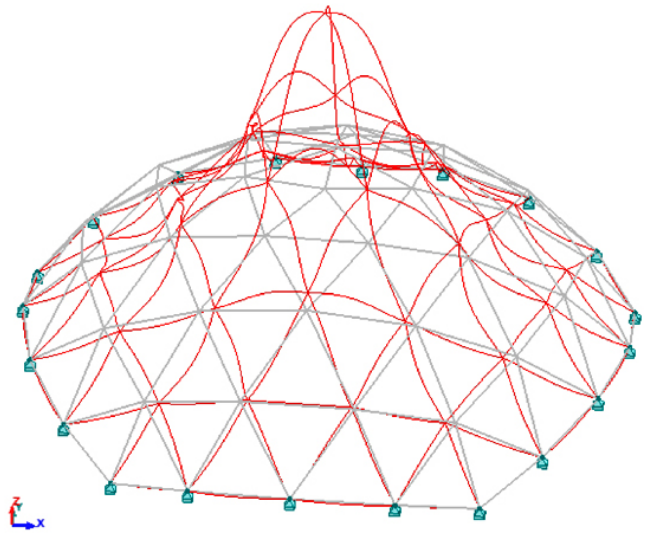

Fig. 7. Graphic illustration of the first mode of vibration of geodesic dome

In order to generate a time-dependent wind speed signal, the Davenport spectrum was used. The wind signal was determined as a sum of sinusoidal components:

$$v(t) = v_0 + \sum_{i=1}^{n} A_i \cdot \sin(2\pi f_i t + \emptyset_i) \tag{3.3}$$

where: $v(t)$ – wind speed over time t, v_0 – average wind speed value, A_i – amplitude of the i-th component, f_i – frequency of the i-th component, $\emptyset_i$ – random phase shift of the i-th component, n – number of harmonic components.

To determine the wind signal, it is necessary to take into account the initial assumptions. In the considered case, the following were taken into account: average wind speed $U = 25$ m/s, standard deviation of turbulence as: $\sigma_U = 2$ m/s, integral length of turbulence $L = 100$ m. The frequency range from 0 to 2 Hz was assumed, taking into account the division into 8 harmonic components. Table 2 presents the determined values of the power spectrum, amplitude and an

example random phase for the adopted assumptions. For further assumptions, it was necessary to assume one set of randomly selected values of random phases. Figure 8 shows a graph of the generated wind speed signal over time.

Table 2. Results of power spectral density, amplitude and example random phase

Frequency f_i [Hz]	**Power spectral density [m/s^2]**	**Amplitude [m]**	**Example random phase [rad]**
0.000	64.000	5.657	1.518
0.250	2.499	1.118	4.871
0.500	0.890	0.667	3.451
0.750	0.473	0.486	2.078
1.000	0.299	0.387	5.821
1.250	0.209	0.323	2.594
1.500	0.156	0.279	0.161
1.750	0.121	0.246	3.047

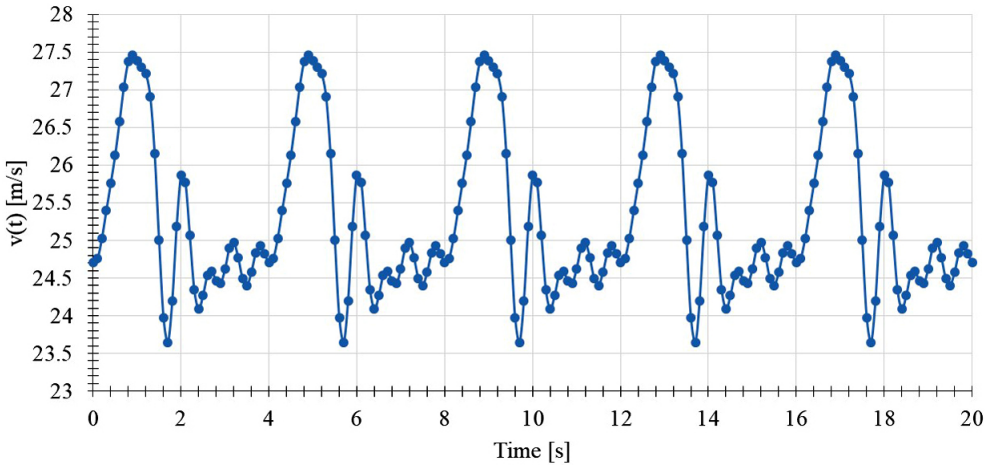

Fig. 8. Wind speed signal generated over time

Figures 9 and 10 show the change of the vertical displacement value in the keystone of geodesic and Schwedler dome. Figures 11 and 12 show the dynamic acceleration in the vertical direction in the keystone of the geodesic dome and Schwedler dome. In designing such structures, the values of axial forces in the most stressed bars are crucial. The final figures (Figures 13 and 14) show the dynamic variations of these forces. We can observe that the character of these graphs is similar to that of the vertical displacements. Moreover, during the dome's movement, the bars are alternately compressed and tensioned. This is particularly dangerous for bars initially designed for tension.

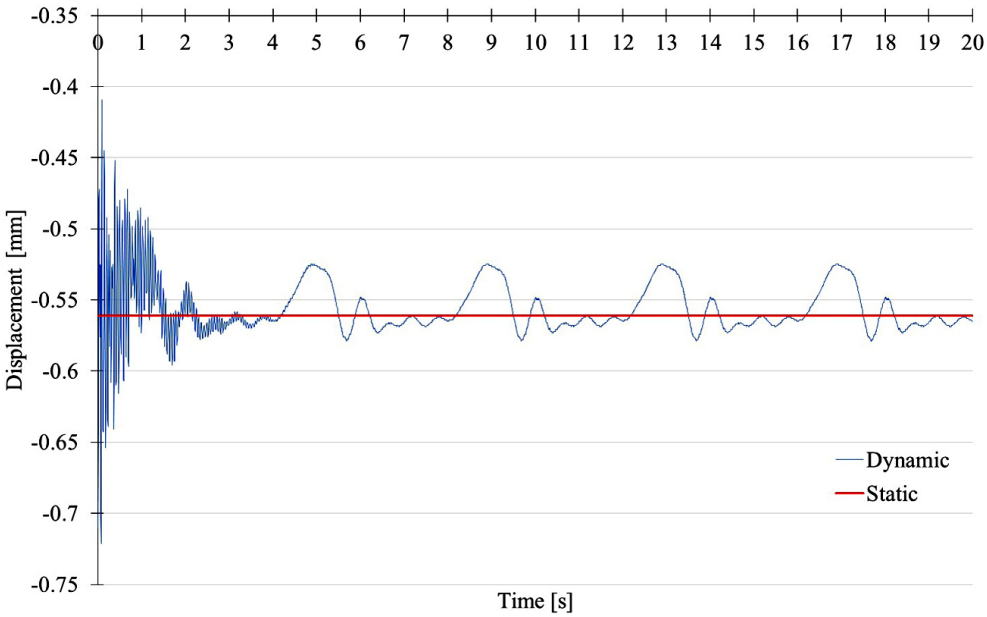

Fig. 9. Dynamic course of vertical displacement in the keystone of the geodesic dome

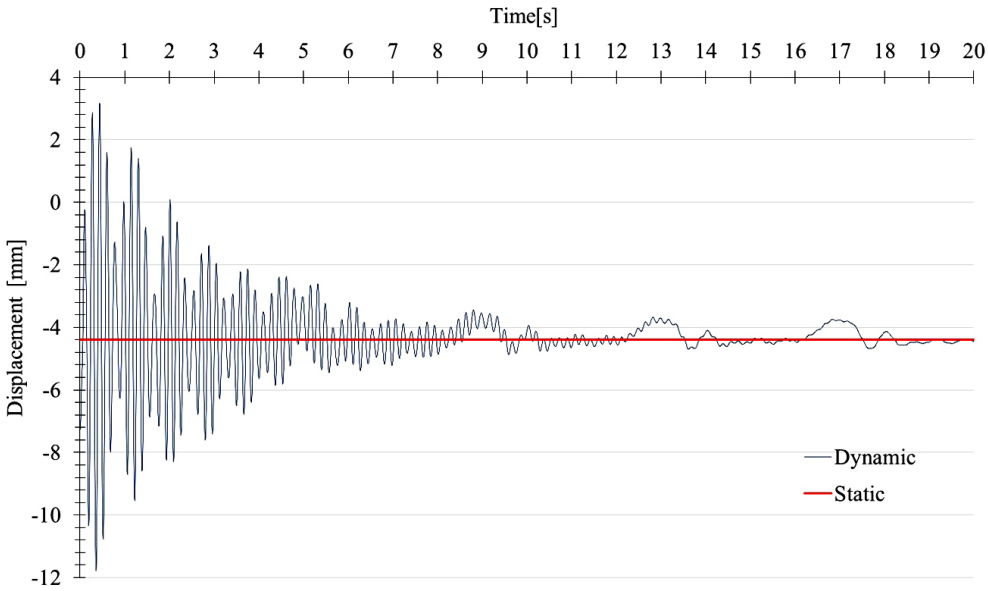

Fig. 10. Dynamic course of vertical displacement in the keystone of the Schwedler dome

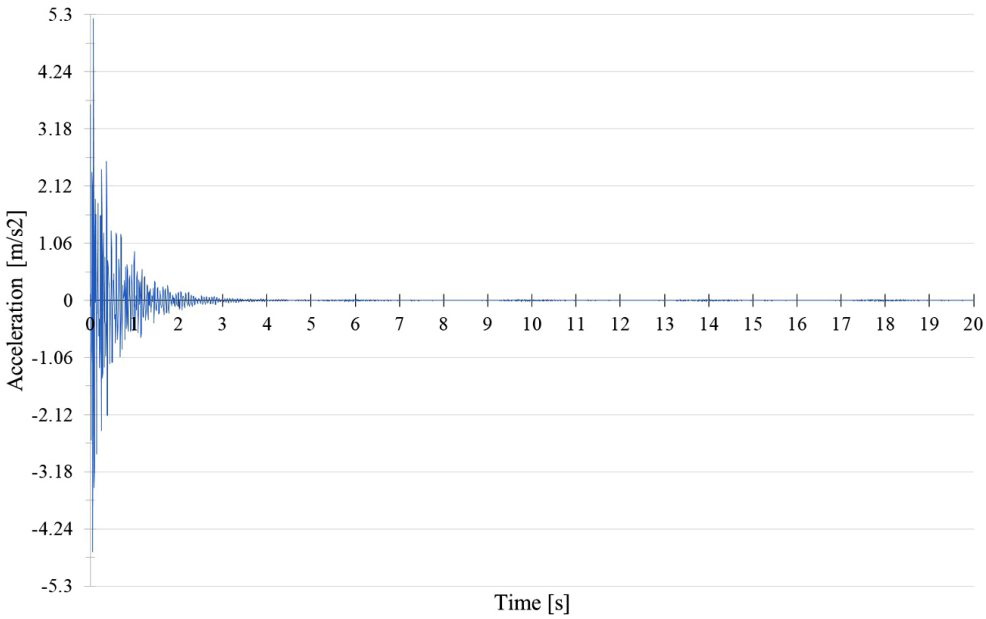

Fig. 11. Dynamic acceleration in the vertical direction in the keystone of the geodesic dome

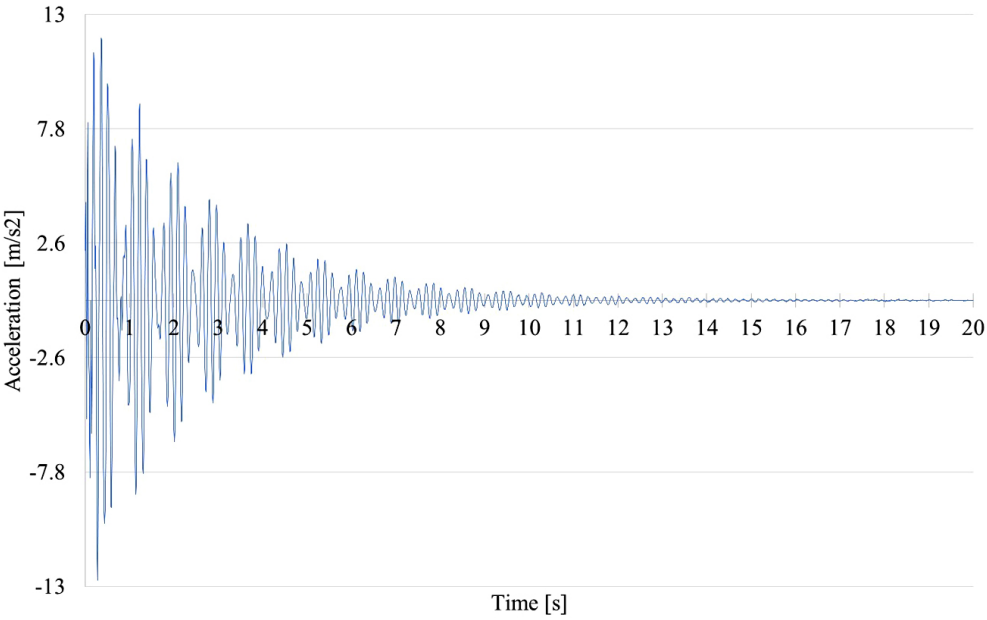

Fig. 12. Dynamic acceleration in the vertical direction in the keystone of the Schwedler dome

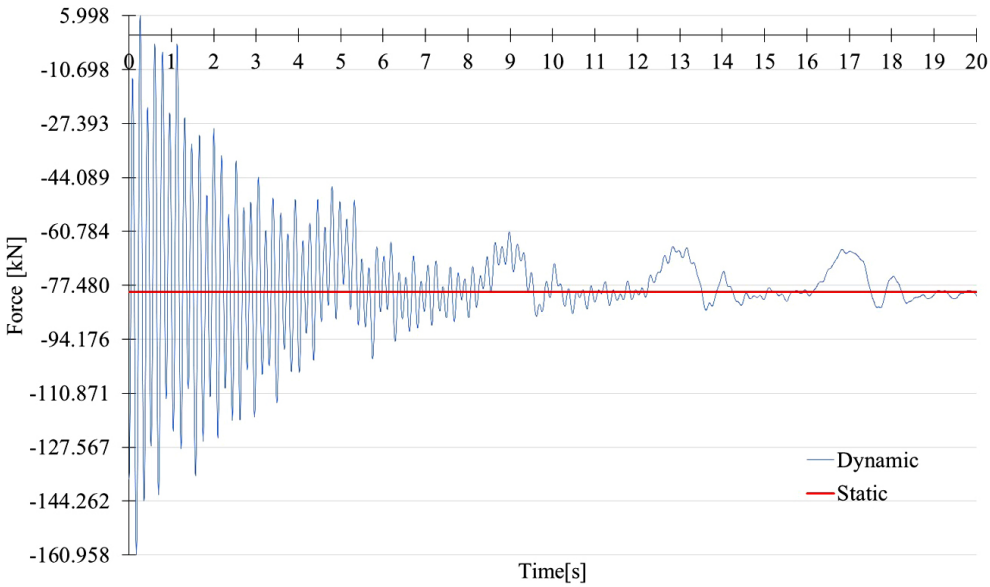

Fig. 13. Dynamic course of the axial force in bar no. 40 of the Schwedler dome

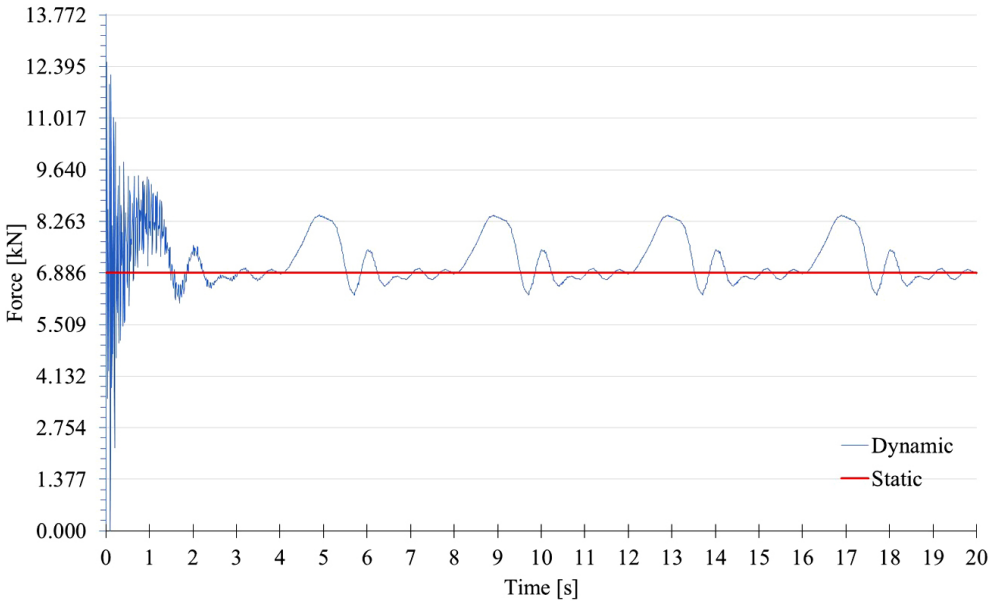

Fig. 14. Dynamic course of the axial force in bar no. 75 of the geodesic dome

4. Discussion and conclusions

In accordance with the applicable standards, we design dome-shaped roofs assuming that each load is a static load. The authors decided to check how each dome would behave under the influence of sudden changes of the load value. The domes differ in geometry. Schwedler's dome is a low-rise structure, characterized by very high flexibility. For this dome, the height-to-span ratio is 0.04. The opposite of the Schwedler dome is a geodesic dome which the height to span ratio is 0.31. Due to its low stiffness, the Schwedler dome is very susceptible to dynamic influences. It is worth noting that it also dampens vibrations poorly. The geodesic dome achieves several times lower values of displacements, accelerations and axial forces, and perfectly silences oscillations. The main aim of this paper was comparing results obtained from the application of dynamic equilibrium equations and those derived from static analysis. Observing the values of the force in bar number 75 of the geodesic dome, we can see that it changes sign during vibrations. The steel bar originally designed as tension is forced to take over compressive stresses. However, the situation described does not last long. The geodesic dome perfectly dampens vibrations and we quickly return to the initial situation. In the case of the Schwedler dome, we are not so lucky. The damping capacity of the Schwedler dome is definitely weaker. The most stressed member in the Schwedler dome, originally designed to resist a compressive force of 79.5 kN, is required to carry a load nearly twice as high – 160.9 kN. The probability of buckling of the bar during the described situation is very high. The potential for damage to the trapezoidal metal sheets of the Schwedler dome, due to a large range of displacements (from –11.8 mm to 3.2 mm), is also a non-negligible factor. The influence of variable displacements and axial forces on the structural performance of a bar-type roof structure – particularly under dynamic wind loading – is significant in terms of both structural safety and durability. Cyclic deformations may lead to material fatigue, especially in joints and welds. Movements can weaken connections (e.g., bolts, welds), which over time may result in loosening or damage. Taking dynamic effects into account can be of fundamental importance in the design process of these types of structures.

References

[1] W.A.H. Mashrah, B. Rima, H. Liu, Z. Chen, and B. Fu, "Static stability analysis of steel single-layer spherical latticed shells with and without roofing systems", *Journal of Building Engineering*, vol. 77, art. no. 107141, 2023, doi: 10.1016/j.jobe.2023.107141.

[2] X. Cui, Y. Li, and H. Hong, "Reliability of stability of single-layer latticed shells with spatially correlated initial geometric imperfection modeled using conditional autoregressive model", *Engineering Structures*, vol. 201, art. no. 109787, 2019, doi: 10.1016/j.engstruct.2019.109787.

[3] K. Kubicka and U. Radoń, "Influence of the buckling coefficient randomness on the reliability index value under fire conditions", *Archives of Civil Engineering*, vol. 64, no. 3, pp. 173–179, 2018.

[4] A. Kaveh and S. Talatahari, "Geometry and topology optimization of geodesic domes using charged system search", *Structural and Multidisciplinary Optimization*, vol. 43, no. 2, pp. 215–229, 2011, doi: 10.1007/s00158-010-0566-y.

[5] H. Wu, Y. Wu, P. Zhi, X. Wu, and T. Zhu, "Structural optimization of single-layer domes using surrogate-based physics-informed neural networks", *Heliyon*, vol. 9, no. 10, 2023, doi: 10.1016/j.heliyon.2023.e20867.

[6] A. Bigham and S. Gholizadeh, "Topology optimization of nonlinear single-layer domes by an improved electro-search algorithm and its performance analysis using statistical tests", *Structural and Multidisciplinary Optimization*, vol. 62, no. 4, pp. 1821–1848, 2020, doi: 10.1007/s00158-020-02578-4.

[7] G. Nie, X. Zhi, F. Fan, and J. Dai, "Seismic performance evaluation of single-layer reticulated dome and its fragility analysis", *Journal of Constructional Steel Research*, vol. 100, pp. 176–182, 2014, doi: 10.1016/j.jcsr.2014.04.031.

[8] Z. Zhu, Y. Xiang, Y. Peng, and Y. Luo, "Earthquake-induced collapse of steel latticed shell: energy criterion implementation and experimental validation", *Engineering Structures*, vol. 236, art. no. 112102, 2021, doi: 10.1016/j.engstruct.2021.112102.

[9] P. Li, G. Chen, H. Lu, L. Ke, H. Wang, and B. Jian, "Dynamic responses of single-layer reticulated shells under oblique impact loading", *Buildings*, vol. 14, no. 3, art. no. 633, 2024, doi: 10.3390/buildings14030633.

[10] W. Lu, J. Wang, H. Guo, H. Li, and J. Sun, "Wind-induced dynamic collapse analysis of single-layer cylindrical reticulated shells considering roof slabs and support columns", *International Journal of Heat and Technology*, vol. 38, no. 1, pp. 180–186, 2020, doi: 10.18280/ijht.380120.

[11] A. Alizadeh and B. Shekastehband, "Wind-induced instability analysis of large-span single-layer lattice domes", *Thin-Walled Structures*, vol. 181, art. no. 110109, 2022, doi: 10.1016/j.tws.2022.110109.

[12] M. Majowiecki, "Structural Architecture of Wide Span Enclosures: Uncertainties in Reliability Assessment", presented at 5°Conference on Metal Structures, 29.09-02.10.2005, Xanthi, 2005.

[13] S. Bachmeier, "Reno, Nevada radar dome failure", CIMSS Satellite Blog. [Online]. Available: https://cimss.ssec.wisc.edu/satellite-blog/archives/1581. [Accessed 13 Jul. 2023].

[14] P. Obara, M. Solovei, and J. Tomasik, "Parametric dynamic analysis of tensegrity cable-strut domes", *Journal of Theoretical and Applied Mechanics*, vol. 62, no. 2, pp. 253–267, 2024.

[15] P. Obara and M. Solovei, "Influence of the initial prestress level on the distribution of regions of dynamic instability of Geiger domes", *Applied Sciences*, vol. 14, no. 17, art. no. 7512, 2024, doi: 10.3390/app14177512.

[16] M. Solovei and P. Obara, "Assessment of the impact of the number of girders on the dynamic behaviour of Geiger dome", *Archives of Civil Engineering*, vol. 69, no. 3, pp. 597–611, 2023, doi: 10.24425/ace.2023.146100.

[17] V. Alpatov, O. Veremeenko, A. Sakharov, and V. Shirokov, "Trial design of a dome roof for a church", *MATEC Web of Conferences*, vol. 86, art. no. 02015, 2016, doi: 10.1051/matecconf/20168602015.

[18] K. Jeleniewicz, J. Jaworski, M. Żółtowski, I. Uziębło, A. Stefańska, and S. Dixit, "Steel ribbed dome structural performance with different node connections and bracing system", *Scientific Reports*, vol. 14, art. no. 14013, 2024, doi: 10.1038/s41598-024-64811-0.

[19] P. Zabojszcza, U. Radoń, and W. Szaniec, "Probabilistic approach to limit states of a steel dome", *Materials*, vol. 14, no. 19, art. no. 5528, 2021, doi: 10.3390/ma14195528.

[20] A. Dudzik and B. Potrzeszcz-Sut, "Hybrid approach to the First Order Reliability Method in the reliability analysis of a spatial structure", *Applied Sciences*, vol. 11, no. 2, art. no. 648, 2021, doi: 10.3390/app11020648.

[21] B. Potrzeszcz-Sut, "Reliability analysis of shell truss structure by hybrid Monte Carlo method", *Journal of Theoretical and Applied Mechanics*, vol. 58, no. 2, pp. 469–482, 2020.

[22] X. Lu, S. Chen, X. Zhao, and X. Lu, "Lectotype optimization of single-layer steel reticulated dome based on BP neural network method", in *Proceedings of the 7th International Conference on Fuzzy Systems and Knowledge Discovery*. IEEE, 2010, vol. 5, pp. 2100–2104, doi: 10.1109/FSKD.2010.5569715.

[23] M. Zhang, Y. Liu, Z. Yu, and G. Parke, "Study of seismic resistance of Kiewit-8 dome considering key structural design parameters", *Advanced Steel Construction*, vol. 15, no. 4, pp. 386–397, 2019, doi: 10.18057/IJASC.2019.15.4.9.

[24] G. Kiewitt, "Roof structure", U.S. Patent No. 2,908,236, 1959.

[25] A. Manguri, N. Saeed, F. Kazemi, N. Asgarkhani, and R. Jankowski, "The effect of minimum actuation limit in shape control of a single-layer dome frame", *Eurasian Journal of Science and Engineering*, vol. 10, no. 1, pp. 77–88, 2024, doi: 10.23918/eajse.v10i1p7.

[26] U. Radoń, P. Zabojszcza, and M. Sokol, "The influence of dome geometry on the results of modal and buckling analysis", *Applied Sciences*, vol. 13, no. 4, art. no. 2729, 2023, doi: 10.3390/app13042729.

[27] D. Opatowicz, U. Radoń, and P. Zabojszcza, "Assessment of the effect of wind load on the load capacity of a single-layer bar dome", *Buildings*, vol. 10, no. 10, art. no. 179, 2020, doi: 10.3390/buildings10100179.

[28] R. Fuller, "Geodesic domes", U.S. Patent No. 2,682,235, 1962.

[29] R. Fuller, "Tensile-integrity structures", U.S. Patent No. 3,063,521, 1967.

[30] R. Fuller, "Octahedronal building truss", U.S. Patent No. 3,354,591, 1969.

[31] P. Zabojszcza and U. Radoń, "Effect of increased density of nodes in geodesic dome on its critical load capacity", *IOP Conference Series: Materials Science and Engineering*, 2019, vol. 471, art. no. 052051, doi: 10.1088/1757-899X/471/5/052051.

[32] L. Carassale, G. Piccardo, and G. Solari, "Double modal transformation and wind engineering applications", *Journal of Engineering Mechanics*, vol. 127, no. 5, pp. 411–529, 2001, doi: 10.1061/(ASCE)0733-9399(2001)127:5(432).

[33] Y. Uematsu, M. Yamada, A. Inoue, and T. Hongo, "Wind loads and wind-induced dynamic behavior of a single-layer latticed dome", *Journal of Wind Engineering and Industrial Aerodynamics*, vol. 66, no. 3, pp. 227–248, 1997, doi: 10.1016/S0167-6105(97)00133-5.

[34] H. Pan, L. Xie, and J. Fu, "Estimation of wind load on supertall buildings using partial output measurements", *Engineering Structures*, vol. 310, art. no. 118141, 2024, doi: 10.1016/j.engstruct.2024.118141.

[35] A. Davenport, "The spectrum of horizontal gustiness near the ground in high winds", *Quarterly Journal of the Royal Meteorological Society*, vol. 87, pp. 194–211, 1961, doi: 10.1002/qj.49708737208.

[36] E. Simiu and R. Scanlan, *Wind Effects on Structures: Fundamentals and Applications to Design*. John Wiley & Sons, 1996.

[37] N. Newmark, "A method of computation for structural dynamics", *Journal of the Engineering Mechanics Division*, vol. 85, no. 3, pp. 67–94, 1959, doi: 10.1061/JMCEA3.0000098.

[38] Numpress Computer System. [Online]. Available: http://www.numpress.ippt.pan.pl (in Polish).

[39] P. Zabojszcza and U. Radoń, "The impact of node location imperfections on the reliability of single-layer steel domes", *Applied Sciences*, vol. 9, no. 13, art. no. 2742, 2019, doi: 10.3390/app9132742.

[40] P. Zabojszcza and U. Radoń, "Stability analysis of the single-layer dome in probabilistic description by the Monte Carlo method", *Journal of Theoretical and Applied Mechanics*, vol. 58, no. 2, pp. 425–436, 2020.

[41] LAPACK – Linear Algebra PACKage. [Online]. Available: https://www.netlib.org/lapack/.

[42] G. Rakowski, Ed. *Mechanika budowli. Ujęcie komputerowe*, vol. 2. Warszawa: Wydawnictwo Arkady, 1992.

List of standards:

N.1. EN 1990: 2002 Eurocode – Basis for structural design.
N.2. EN 1991-1-3 Eurocode 1: Actions on structures – Part 1–3: General actions – Snow loads.
N.3. EN 1991-1-4 Eurocode 1: Actions on structures – Part 1–4: General actions – Wind actions.
N.4. EN 1993-1-1 Eurocode 3: Design of steel structures – Part 1–1: General rules and rules for buildings.

Odpowiedzi dynamiczne kopuły Schwedlera i geodezyjnej na obciążenie wiatrem

Słowa kluczowe: obciążenie wiatrem, analiza modalna, metoda Newmarka, kopuła Schwedlera, kopuła geodezyjna

Streszczenie:

W wielu zagadnieniach inżynierskich wystarczy traktować wiatr jako obciążenie statyczne. W tych statycznych obliczeniach prędkość wiatru jest stała. Niestety, w przypadku konstrukcji podatnych, podmuchy wiatru mogą powodować drgania o znacznych amplitudach. Aby obliczyć siłę wiatru, konieczne jest wówczas prawidłowe określenie zależności opisującej, jak prędkość wiatru zmienia się w zależności od czasu i położenia. Zależność prędkości wiatru można przedstawić jako sumę średniej prędkości wiatru i losowych fluktuacji. Losowe fluktuacje prędkości wiatru są charakteryzowane w dziedzinie

częstotliwości przez funkcję gęstości widmowej. W analizach dynamicznych wykorzystujemy model wiatru oparty na szeregu Fouriera, który przedstawia zmienność prędkości wiatru w czasie jako sumę kilku prostych fal sinusoidalnych, czyli składowych harmonicznych. Każda z nich ma swoją częstotliwość, amplitudę i fazę początkową. Każda składowa harmoniczna odpowiada za inny „rytm" zmian wiatru – np. jedna za wolne fluktuacje, inna za szybkie drgania. Dodając je wszystkie razem, otrzymujemy przebieg wiatru zbliżony do rzeczywistego. Taki model jest przydatny np. w analizie dynamicznej stalowych pokryć dachowych, gdzie konieczne jest uwzględnienie działania wiatru zmieniającego się w czasie w bardziej uporządkowanej i przewidywalnej formie. W naszej pracy parametry dla każdej fali sinusoidalnej są obliczane przy użyciu funkcji gęstości widmowej Davenporta. Autorzy postanowili sprawdzić, jak każda kopuła zachowa się pod wpływem nagłych zmian wartości obciążenia. Kopuły różnią się geometrią. Kopuła Schwedlera jest konstrukcją niską, charakteryzującą się bardzo dużą elastycznością. Dla tej kopuły stosunek wysokości do rozpiętości wynosi 0,04. Przeciwieństwem kopuły Schwedlera jest kopuła geodezyjna, której stosunek wysokości do rozpiętości wynosi 0,31. Ze względu na małą sztywność kopuła Schwedlera jest bardzo podatna na wpływy dynamiczne. Warto zauważyć, że słabo tłumi również drgania. Kopuła geodezyjna osiąga kilkukrotnie niższe wartości przemieszczeń, przyspieszeń i siłosiowych oraz doskonale tłumi drgania. Głównym celem niniejszej pracy było porównanie wyników uzyskanych z zastosowania równań równowagi dynamicznej i tych wyprowadzonych z analizy statycznej. Obserwując wartości siły w pręcie nr 75 kopuły geodezyjnej, możemy zobaczyć, że zmienia ona znak podczas drgań. Pręt stalowy pierwotnie zaprojektowany jako rozciągany jest zmuszony przejąć naprężenia ściskające. Jednak opisana sytuacja nie trwa długo. Kopuła geodezyjna doskonale tłumi drgania i szybko wracamy do sytuacji początkowej. W przypadku kopuły Schwedlera nie mamy tyle szczęścia. Zdolność tłumienia kopuły Schwedlera jest zdecydowanie słabsza. Najbardziej obciążony element kopuły Schwedlera, pierwotnie zaprojektowany do wytrzymywania siły ściskającej 79,5 kN, musi przenosić obciążenie prawie dwukrotnie większe – 160,9 kN. Prawdopodobieństwo wyboczenia pręta podczas opisanej sytuacji jest bardzo wysokie. Potencjalne uszkodzenie blach trapezowych kopuły Schwedlera, ze względu na duży zakres przemieszczeń (od –11,8 mm do 3,2 mm), jest również czynnikiem nie do pominięcia. Wpływ zmiennych przemieszczeń i siłosiowych na parametry konstrukcyjne konstrukcji dachu prętowego – szczególnie pod wpływem dynamicznego obciążenia wiatrem – jest znaczący zarówno pod względem bezpieczeństwa konstrukcyjnego, jak i trwałości. Cykliczne odkształcenia mogą prowadzić do zmęczenia materiału, zwłaszcza w połączeniach i spoinach. Ruchy mogą osłabiać połączenia (np. śruby, spoiny), co z czasem może prowadzić do poluzowania lub uszkodzenia. Uwzględnienie efektów dynamicznych może mieć fundamentalne znaczenie w procesie projektowania tego typu konstrukcji.

Received: 2025-06-12, Revised: 2025-07-24